Turbulent Spectrum of the Earth's Ozone Field

L. Sirovich, R. Everson, and D. Manin
The Rockefeller University, New York, New York 10021
(Received 11 May 1994)

The total ozone mapping spectrometer database is subjected to an analysis in terms of the Karhunen-Loève empirical eigenfunctions. The concentration variance spectrum is transformed into a wave-number spectrum, $E_c(k)$. In terms of the wave number, $E_c(k)$ is shown to be $O(k^{-2/3})$ in the inverse cascade regime, and $O(k^{-2})$ in the enstrophy cascade regime with the spectral *knee* at the wave number of baroclinic instability. The spectrum is related to known geophysical phenomena and shown to be consistent with physical dimensional reasoning for the problem. The appropriate Reynolds number for the phenomena is Re $\approx 10^{10}$.

PACS numbers: 94.10.Fa, 47.27.Jv

Atmospheric mixing is effected at horizontal scales which are large compared with the scale height ($\approx$10 km), which with inhibition of vertical motion by planetary rotation and stable stratification contributes to the two-dimensional picture of atmospheric activity [1,2]. In addition to its essential role in meteorology, current interest in mixing is enhanced by its role in regard to the behavior of the Antarctica ozone *hole* [3] and to the lack of such an *effect* in the Arctic [4].

Our investigation is based on satellite records of the earth's ozone fields. We have analyzed fifteen years of daily ozone fields of the TOMS (total ozone mapping spectrometer) database [5]. Because of technical and natural causes, each daily record contains gaps in the form of missing pixels. A typical snapshot appears in Fig. 1. The dark regions represent areas of missing pixels caused partly by technical failure and in part due to polar night (measurements are based on reflected light). Each record is *stitched* together from sixteen separate records obtained from south-north synchronous orbits that are taken in a 24 h period from the satellite, Nimbus.

Such a large data set recommends a statistical analyses, and we focus on spectral properties of the ozone field. Although ozone production (equatorial regions) and depletion (polar regions) result from complex chemical reactions [6], these represent relatively weak sources and sinks, and we follow common practice and regard ozone as a passive scalar. The variance spectrum of a scalar contaminant in turbulent flows has been recently reviewed by Sreenivasan [7]. Functional estimates for the concentration variance spectrum (in homogeneous isotropic turbulence) follow from dimensional arguments based on those first given by Kolmogorov, leading to the famous $E_K(k) = K\epsilon^{2/3}k^{-5/3}$ energy spectrum for the inertial range [8].

Obukhov and co-workers [9] show that an inertial range can exist, in particular, the variance per wave number of concentration, c, denoted by $E_c(k)$, has the form

$$E_c(k) = C\chi\epsilon^{-1/3}k^{-5/3}, \tag{1}$$

where C is a dimensionless constant, ϵ is the usual turbulent energy transport rate, and $\chi = \langle\kappa(\nabla c)^2\rangle$ is the appropriate *dissipation* rate. Thus the concentration spectrum appears tied to the corresponding velocity spectrum. Experimental observations [7] show departures from the universal form (1), except at very high Reynolds numbers. For small diffusional effects, Batchelor [10] has shown that $E_c = O(k^{-1})$. This holds under a less restrictive

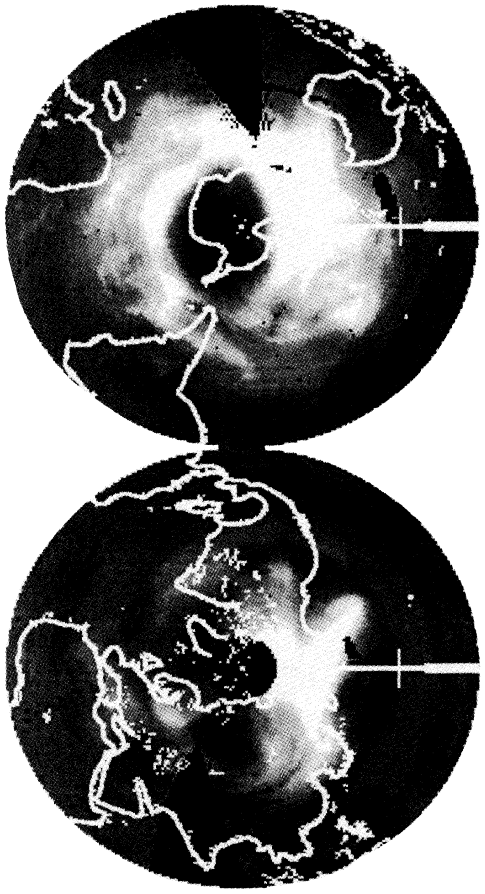

FIG. 1. Typical statellite image of the global atmospheric ozone field. The grayscale indicates the total ozone in a column above each location. Missing data is shown as black.

0031-9007/95/74(13)/2611(4)$06.00

hypothesis. [11,12]. Except for a recent simulation [12], confirmation of this result has been elusive. Predictions of anomalous scalings have also appeared [13].

Arguments leading to the above spectra are unaltered when applied to two-dimensional turbulence. However, the interpretation of the cascade of energy represented by the spectrum $E_K(k)$ requires some additional remarks. Both energy E and enstrophy $\Omega = \int(\nabla \wedge \mathbf{u})^2 d\mathbf{x}$ are inviscid invariants in two dimensions. As a result of this, Kraichnan and Batchelor [14] have shown that the Kolmogorov spectrum, E_K, represents an inverse cascade of energy from smaller to larger scales, and that there also exists a second cascade from small k to large k given by the enstrophy $\Omega(k) = C_0\chi_0 k^{-1}$ (with log correction) and hence an energy spectrum $E(k) \propto k^{-3}$, where C_0 is a dimensionless constant and $\chi_0 = \nu\overline{(\nabla\omega)^2}$ (also see [15]). Support for $E = O(k^{-3})$ comes from many direct simulations [16]. However, recent very large scale simulations show substantial divergence in the $O(k^{-5/3})$ inverse cascade range [17]. Observational data from the atmosphere are not definitive, and although a power law energy spectrum is indicated in the enstrophy range, the exponent appears to lie between -2 and -3 [18]. In particular, Schoeberl and Bacmeister [18] suggest that the exponent is -2 down to scales in the 10 km range.

A difficulty in interpreting these results for E_c now appears. For k large, it might be supposed in analogy with three dimensions, that $E_c(k) = O(k^{-3})$; i.e., it should follow the energy spectrum. On the other hand, the vorticity (a scalar) formally satisfies the same convection equation as a passive scalar, and one might suppose that $E_c = O(k^{-1})$, the Batchelor spectrum. As will be seen shortly, neither of these hold in the atmosphere.

Other possible scalings for E_c have appeared in the literature. For quasi-two-dimensional turbulence Falkovich and Medvedev [19] find $E = O(k^{-7/3})$ for large k. Saffman [20], in considering the Burgers equation [21], observed that its solutions are nearly piecewise discontinuous which leads to $E_c = O(k^{-2})$. Pierrehumbert, using concepts from chaotic mixing, has obtained a variety of scalings for E_c from both mathematical and physical models [22].

Satellite images (see Fig. 1) are clearly inhomogeneous, and a transformation to wave-number concepts is required. As will be seen, the Karhunen-Loève (KL) procedure [23] is ideally suited for this purpose. In particular, the snapshot method [24] considerably reduces the needed computational effort. However, the presence of gappy data required modification of the methodology [25]. This, as well as an extensive analysis of the results, appears in Manin, Everson, and Sirovich [26], and a mathematical treatment is also given elsewhere [27].

To connect the usual wave-number spectrum with that obtained from the empirical eigenfunctions, we recall an argument used in another discussion [28]. The concentration fluctuation of ozone is denoted by $c(\mathbf{x}, t)$. For purposes of later dimensional reasoning, we write the dimensions of c as $\dim[c] = m/l^2$, where m refers to molecules (of ozone) per area since the data are two-dimensional. The mean variance in the homogeneous case is given by

$$\overline{c^2} = \frac{1}{A}\int c^2\, d\mathbf{x} = \int \mathcal{E}_c(\mathbf{k})\, d\mathbf{k} = \int E_c(k)\, dk\,. \quad (2)$$

Thus $\dim[\mathcal{E}_c] = m^2 l^{-2}$ and $\dim[E_c] = m^2 l^{-3}$. To treat the inhomogeneous case corresponding to the data, we consider the correlation

$$K_c(\mathbf{x}, \mathbf{y}) = \langle c(\mathbf{x}) c(\mathbf{y})\rangle\,, \quad (3)$$

which from KL can be written in spectral form

$$K_c = \sum_n \lambda_n \psi_n(\mathbf{x})\psi_n(\mathbf{y})\,, \quad (4)$$

where $\{\psi_n\}$ are the eigenfunctions of the operator K_c. The total variance is given by

$$\left\langle \int c^2(\mathbf{x})\, d\mathbf{x} \right\rangle = \mathrm{Tr}K = \sum_n \lambda_n\,. \quad (5)$$

An eigenvalue λ_n represents the average variance allocated to the projection of c onto ψ_n. The summation (5) is the natural generalization of (2) to the inhomogeneous case. Each λ_n represents the variance in a state, thus generalizing $\mathcal{E}_c(\mathbf{k})$, and has the same dimensions,

$$\dim[\lambda] = \dim[\mathcal{E}] = m^2 l^{-2}. \quad (6)$$

In Fig. 2 we display in doubly logarithmic form λ_n versus index n. As is seen, the variance spectrum falls, to good approximation, on two different power laws

$$\lambda_n \propto \begin{cases} n^{\alpha_i};\ n < 35\,, & \alpha_i = 0.85 \pm 0.035\,, \\ n^{\alpha_0};\ n > 50\,, & \alpha_0 = -1.56 \pm 0.022\,. \end{cases} \quad (7)$$

The error bounds appearing in (7) are based only on the least squares fit to the data, and not on the methods used in arriving at the spectrum which appears in Fig. 2. The region of the *knee,* $35 \le n \le 50$, will be discussed below.

In order to relate n to k, we observe that in the homogeneous case modes carrying variances larger than those at k can be counted in number, N, as

$$N \propto k^2, \qquad \text{whence} \quad k \propto N^{1/2}. \quad (8)$$

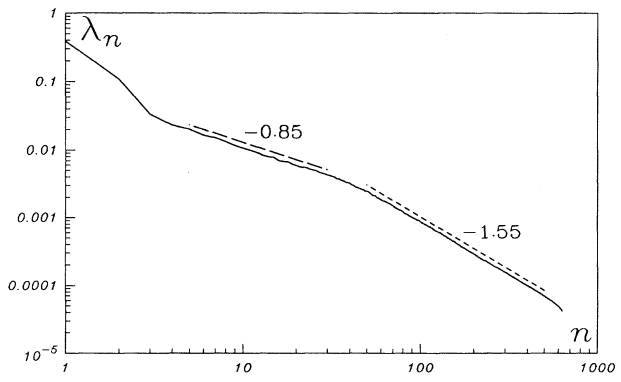

FIG. 2. Eigenvalues, λ_n, from a modified Karhunen-Loève decomposition of 15 year global ozone data set.

Before continuing, it is instructive to verify these relations. For this purpose we employ the inverse relation between wave number and length scale. Thus (8) implies that the length scale, L_n, of the nth eigenfunction bears the following dependence on the index:

$$L_n \propto n^{-1/2}. \tag{9}$$

An informal perusal of the eigenfunctions themselves supports this relationship between characteristic length and index. To quantify this we have computed the correlation length of each eigenfunction [26], and the result is plotted in Fig. 3. It is clear from this figure that (9) provides an excellent fit to the data in the two asymptotic regimes. The region of the *knee* is the only anomaly, and it appears as a plateau in the figure and corresponds to just one scale.

$$2\pi/k_* = L_* \approx 4000 \text{ km}. \tag{10}$$

It is generally stated in the geophysical literature [1,29] that the baroclinic instability gives rise to a pattern of wave number roughly seven; i.e., the unstable pattern is made up of approximately seven pairs of cyclonic/anticyclonic motions. With some indulgence on the part of the viewer, eigenfunction ψ_{44} shown in Fig. 4 appears to have this property. Roughly speaking, each of the eigenfunctions in the range $35 \leq n \leq 50$ shows this spatial arrangement. To explain the plateau in Fig. 3 we suggest an analogy with the von Karman vortex trail. In that case a period seven disturbance requires fourteen independent modes for its description [30]. In view of the nature of the results and the similarity in the number of modes, this would appear to be a reasonable explanation.

The energetics of the atmosphere has its origin in solar heating. However, dynamical activity introduces L_* as the length scale at which mechanical energy is supplied, and is thus the significant length scale of the problem. If ϵ is the energy transport rate which characterizes the inverse energy cascade, then

$$\chi_0 = k_*^2 \epsilon \tag{11}$$

characterizes the enstrophy cascade to higher wave numbers. Using estimates for the physical parameters of the atmosphere and L_* from (10), we obtain the Reynolds number, $R \approx 10^{10}$. Henceforth, we will regard scales smaller than L_* as being in the enstrophy range.

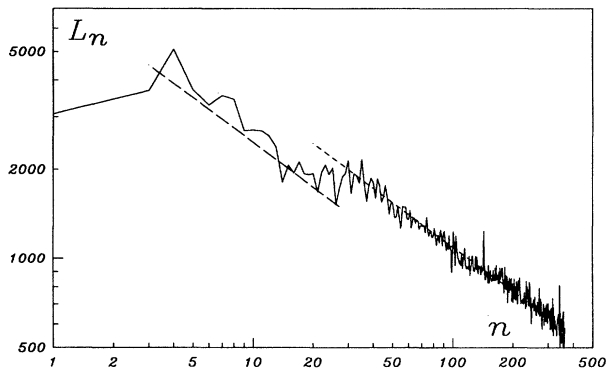

FIG. 3. Correlation length of empirical eigenfunctions plotted against mode number.

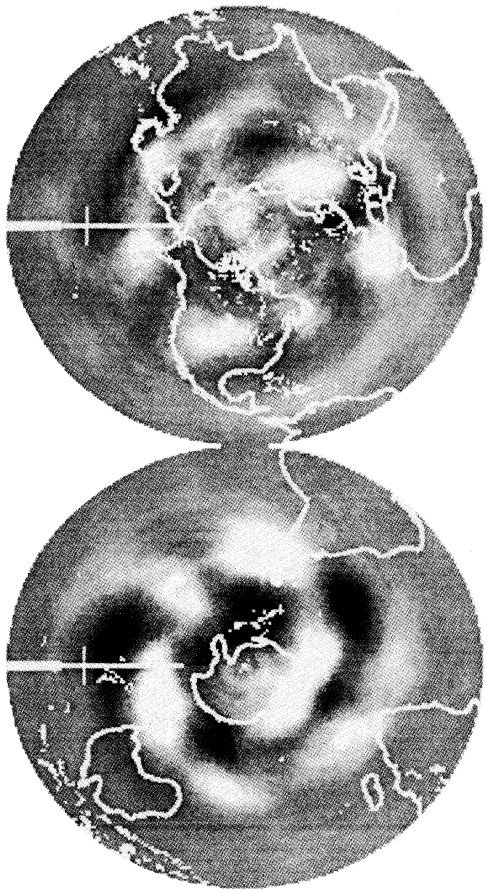

FIG. 4. Empirical eigenfunction, ψ_{44}, displaying the wave number 7, characteristic of the baroclinic instability.

We now return to the implications of the power laws for λ_n (7) to the wave-number spectrum. In keeping with customary practice, we consider the variance per wave number $E_c(k) = k\mathcal{E}_c(k)$. It follows from (7) and (8) that

$$E_c(k) \propto \begin{cases} k^{-2/3}, & k < k_*, \\ k^{-2}, & k > k_*. \end{cases} \tag{12}$$

Specific exponents are entered only for suggestive reasons, and the reader is reminded of the range in Eq. (7). Actually, the second exponent lies slightly outside the error bound. (However, it should be noted that Kraichnan [14] actually estimated the enstrophy falloff as $1/k^3 \ln^{1/3} k$; see also [15].) With the exception of the Saffman-Burgers spectrum [20], theoretical predictions outside the above range are in conflict with (12).

In view of (12), we observe that elementary dimensional analysis yields

$$E_c(k) = \chi \epsilon^{-1/3} k_*^{-5/3} f(k/k_*). \tag{13}$$

Equation (12) implies

$$f(k/k_*) \sim \begin{cases} c_i (k/k_*)^{-2/3}, & k/k_* \ll 1, \\ c_o (k_*/k)^2, & k/k_* \gg 1, \end{cases} \tag{14}$$

where c_i and c_0 are dimensionless constants. Hence

$$E_c(k) \sim \begin{cases} c_i \chi \epsilon^{-1/3} k_*^{-1} k^{-2/3}, & k/k_* \ll 1, \\ c_0 \chi_0^{-1/3} \chi k_* k^{-2}, & k/k_* \gg 1, \end{cases} \quad (15)$$

where the first form is appropriate for the inverse energy cascade and the second form is in a form appropriate for the enstrophy cascade. It should be noted that k_* (or L_*) *does not disappear* under either asymptotic limit. In fact, as the functional form (13) implies, it would be impossible to eliminate this parameter entirely in both limits, in contrast with the Kolmogorov law, (1), in which the integral scale does disappear.

The spectra obtained above covers a wide range. The range $k/k_* < 1$ extends to the 10000 km wavelength limit imposed by dynamics [1,31], and the $k/k_* > 1$ extends down to wavelengths of the order of 100 km, the resolution of the data. Lilly, and Smith and Yakhot [32] have recently suggested that an inverse cascade for $E(k)$ exists for a range of wavelengths greater than 10 km (support for this assertion is found in Nastrom, Gage, and Jasperson, [18], but see Schoeberl and Bacmeister [18]). This is based on the assertion that cumulus cloud activity acts as an energy source. We see no evidence for this, but do not regard this as a contradiction since the resolution of the satellite data is greater than 100 km.

It is of course vexing that much of the theory and numerical experiments (also [33]) discussed earlier do not agree with the observed satellite analysis which we present above. Only the Saffman-Burgers spectrum shows agreement. To test this further we have looked at the "discontinuity" patterns of the data and find that $|\nabla c|^2$ shows filamentous one-dimensional patterns [26]. A possible explanation for such strandlike patterns has been discussed recently. Both satellite observations and computer simulations show the presence of tongues of stratospheric air extending from the tropics to midlatitudes. These result from the breaking of Rossby waves at the edge of the polar vortices [34].

The authors are grateful to P. K. Bhartia, B. W. Knight, V. Yakhot, and G. Falkovich for helpful conversations. This work was supported under a grant from NASA-Goddard (NAG 5-2336).

[1] J. Pedlovsky, *Geophysical Fluid Dynamics* (Springer-Verlag, Berlin, 1979).
[2] N. A. Phillips, Rev. Geophys. **1**, 123-176 (1963).
[3] M. R. Schoeberl, R. S. Stolarski, and A. Kreuger, Geo. Res. Lett. **16**, 377 (1989).
[4] M. H. Proffitt *et al.,* Nature (London) **347**, 31 (1990).
[5] Total Ozone Mapping Spectrometer (TOMS) Data, 1978–1993, edited by P. Grimares and R. McPeters (NASA Goddard Space Flight Center, Greenbelt, 1993).
[6] R. P. Wayne, *Chemistry of Atmospheres* (Oxford University Press, London, 1991).
[7] K. R. Sreenivasan, Proc. R. Soc. London A **434**, 165 (1991).
[8] A. N. Kolmogorov, Dok. Akad. Nauk. SSSR **32**, 19–21 (1941).
[9] A. M. Obukhov, Izv. Acad. Nauk SSSR, Geogr. Geofz. **13**, 58–69 (1949); S. Corrsin, Appl. Phys. **22**, 469 (1954); A. S. Monin and A. Yaglom, *Statistical Fluid Mechanics* (MIT, Cambridge, 1971), Vol. 2.
[10] G. K. Batchelor, J. Fluid Mech. **5**, 113 (1958).
[11] R. H. Kraichnan, Phys. Fluids **11**, 945 (1968).
[12] M. Holzer and E. D. Siggia, Phys. Fluids **6**, 1820 (1994).
[13] A. Polyakov, Nucl. Phys. **B396**, 367 (1993); R. H. Kraichnan, Phys. Rev. Lett. **72**, 1016 (1994).
[14] R. H. Kraichnan, Phys. Fluids **10**, 1417 (1967); G. K. Batchelor, *ibid.* **125**, II–233 (1969).
[15] G. Falkovich and V. Lebedev, Phys. Rev. E **49**, R1800 (1994).
[16] J. C. McWilliams, J. Fluid Mech. **146**, 21 (1984); R. Benzi *et al.,* Europhys. Lett. **3**, 811 (1987); J. Phys. A. **21**, 1221 (1988); G. F. Carnevale *et al.,* Phys. Rev. Lett. **66**, 2735 (1991); U. Frisch and P. Sulem, Phys. Fluids **27**, 1921 (1984); L. Smith and V. Yakhot, Phys. Rev. Lett. **71**, 352 (1993).
[17] V. Borue, Phys. Rev. Lett. **72**, 1475 (1994).
[18] M. R. Schoeberl and J. T. Bacmeister, NATO ASI Series **18**, 135 (1992); D. K. Lilly and E. L. Peterson, Tellus **35A**, 379 (1983); G. D. Nastrom, K. S. Gage, and W. H. Jasperson, Nature (London) **310**, 36–38 (1984).
[19] G. Falkovich and S. Medvedev, Europhys. Lett. **19**, 279 (1992).
[20] P. G. Saffman, Stud. Appl. Math. **50**, 377–383 (1971).
[21] J. M. Burgers, Adv. Appl. Mech. **1**, 171 (1948).
[22] R. T. Pierrehumbert, Geophys. Astrophys. Fluid Dyn. **58**, 285 (1991); R. T. Pierrehumbert, J. Atmos. Sci. **50**, 2462 (1993).
[23] L. Sirovich and R. Everson, Int. J. Supercomputer Applications **6**, 50–68 (1992); G. W. Stewart, SIAM Rev. **35**, (1993); G. Berkooz *et al.,* Annu. Rev. Fluid Mech. **25** (1993).
[24] L. Sirovich, Quarterly of Applied Mathematics **XLV**, 561–590 (1987).
[25] R. Everson and L. Sirovich (to be published); D. Manin, R. Everson, B. Knight, and L. Sirovich (to be published).
[26] D. Manin, R. Everson, and L. Sirovich (to be published).
[27] L. Sirovich, R. Everson, B. Knight, and D. Manin (to be published).
[28] B. Knight and L. Sirovich, Phys. Rev. Lett. **65**, 1356 (1990).
[29] J. T. Houghton, *The Physics of Atmospheres* (Cambridge University Press, Cambridge, U.K., 1977).
[30] L. Sirovich, Phys. Fluids **28**, 2723 (1985).
[31] P. B. Rhines, J. Fluid Mech. **69**, 417 (1975).
[32] D. K. Lilly, J. Atmos. Sci. **46**, 2026 (1989); L. M. Smith and V. Yakhot, J. Fluid Mech. **274**, 115(1994).
[33] E. N. Lorenz, Tellus **21**, 289 (1969); J. G. Charney, J. Atmos. Sci. **28**, 1087 (1971).
[34] A. Plumb, Nature (London) **365**, 489 (1993); W. J. Randal *et al., ibid.* **365**, 533 (1993); D. Waugh, *ibid.* **365**, 535 (1993).

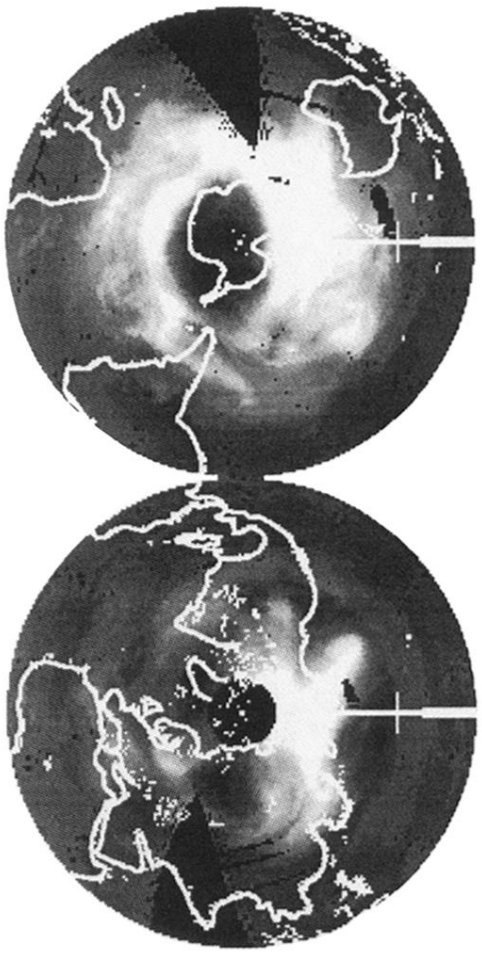

FIG. 1. Typical statellite image of the global atmospheric ozone field. The grayscale indicates the total ozone in a column above each location. Missing data is shown as black.

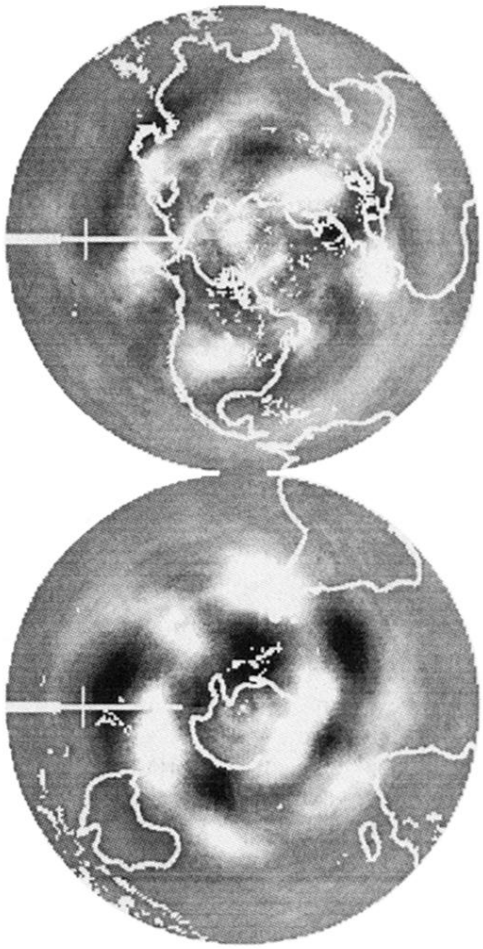

FIG. 4. Empirical eigenfunction, ψ_{44}, displaying the wave number 7, characteristic of the baroclinic instability.